Positron-Annihilation Study of the Electronic Structure of Cu$_{91}$Ge$_9$

P. E. Mijnarends, L. P. L. M. Rabou, and K. E. H. M. Hanssen

Netherlands Energy Research Foundation ECN, 1755 ZG Petten, The Netherlands

and

A. Bansil

Department of Physics, Northeastern University, Boston, Massachusetts 02115
(Received 30 April 1987)

A novel effect of alloying on the electron momentum density in a disordered a-Cu$_{91}$Ge$_9$ alloy is reported. The effect, which is the appearance of a bump in the derivative spectra at low momenta, is predicted by theory employing the coherent-potential approximation and is observed in two-dimensional angular correction experiments on the alloy. It reflects the presence of an s-p impurity band far below the Fermi level. Accurate experimental values for the Fermi-surface radii k_{100} and k_{110} and for the associated disorder-induced smearings in CuGe are also reported for the first time.

Numerous calculations[1] and measurements of the angular correlation of annihilation radiation in two dimensions (2D-ACAR)[2] in pure Cu have established that the momentum density $\rho(\mathbf{p})$ within the Fermi surface (FS) in the first Brillouin zone is flat and featureless. This Letter reports the results of a combined experimental and theoretical study in which we focus on the low-momentum behavior of $\rho(\mathbf{p})$ in Cu$_{91}$Ge$_9$; we find a new structure in the alloy which is absent in Cu. Because of Fourier-transform properties, $\rho(\mathbf{p})$ at low $\mathbf{p}$ directly reflects the properties of s-p states near $\mathbf{k}=0$; these states lie well below (≈ 10 eV) the Fermi level E_F in Cu and Cu-based solid solutions. These states and the associated valence-band edges have not been accessible in previous experiments; for example, in photoemission they possess rather small intensities and are masked by secondary and background emissions. This is the first time that alloying effects originating in states far below E_F have been found to produce a clear signature in $\rho(\mathbf{p})$ and 2D-ACAR spectra.

We have also analyzed our data to obtain FS radii k_{100} and k_{110} with accuracies which in pure Cu approach those obtainable in de Haas–van Alphen (dHvA) experiments. The disorder-induced dampings in the alloy at the FS are reported; here again we are not aware of a

previous direct measurement of this quantity.

The measurements were performed on a 2D-ACAR setup[3] employing position-sensitive detectors of the high-density multiwire-chamber type.[4] After correction for the instrumental response, the measurements yield a
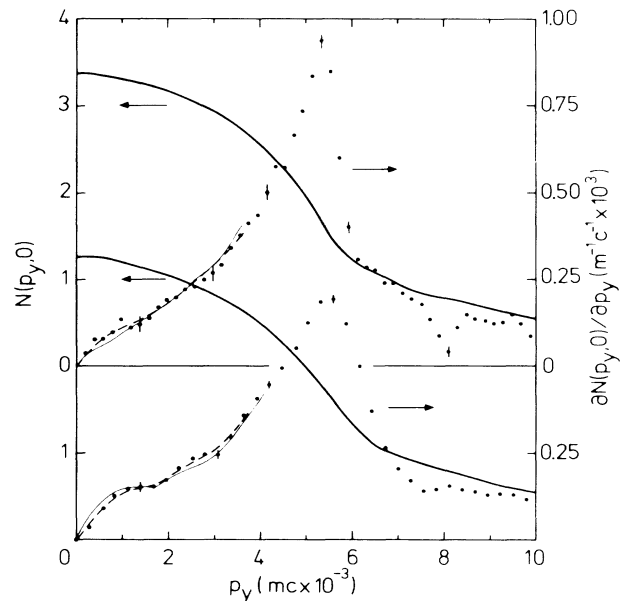

FIG. 1. Cuts along $p_y=[010]$ through the experimental 2D-ACAR distributions (solid lines) with $p_x=[100]$ in Cu (top) and Cu$_{91}$Ge$_9$ (bottom). Five (Cu) or three (Cu$_{91}$Ge$_9$) rows of bins parallel to p_y have been added to improve statistics. The dots give the derivatives obtained from a third-degree least-squares polynomial fit to five successive data points; the more heavily smoothed dashed curves show the low-p behavior more clearly. The thin solid curves at low momenta give the theoretical derivatives (see text).

TABLE I. Sample temperature, instrumental resolution (including positron motion), and bin size in the experiment.

Sample	Temperature (K)	Resolution[a] $[p_y \times p_z]$ (mrad^2)	Bin size[a] (mrad^2)
Cu	8	0.4×0.3	0.198×0.198
Cu$_{91}$Ge$_9$	28	0.6×0.5	0.280×0.280

[a]1 mrad $= 10^{-3}mc$, where m is the electronic rest mass and c the velocity of light.

2D-ACAR distribution given by

$$N(p_y, p_z) = \text{const} \times \int \rho(\mathbf{p}) dp_x. \qquad (1)$$

Here $\rho(\mathbf{p})$ is the two-photon momentum density distribution and p_x the component of $\mathbf{p}$ along the line connecting the detectors. The samples were carefully annealed single crystals of Cu and $Cu_{91}Ge_9$, oriented with p_x within 1° of first the [100] and then the [1$\bar{1}$0] direction. The experimental parameters are summarized in Table I.

Figure 1 shows cuts along $p_y = [010]$ through the Cu and alloy 2D-ACAR distributions, together with their derivatives. The appearance of a bump in the low-momentum region $[(0-2) \times 10^{-3} mc]$ of the alloy derivative spectrum (lower part of Fig. 1) is clearly evident.

To understand the origin of this bump we have computed $\rho(\mathbf{p})$ in Cu and the configurational average $\langle\rho(\mathbf{p})\rangle$ in $Cu_{90}Ge_{10}$ with a constant positron wave function. $\langle\rho(\mathbf{p})\rangle$ was calculated in the Korringa-Kohn-Rostoker coherent-potential approximation (KKR-CPA).[5-7] Figure 2 shows that $\langle\rho(\mathbf{p})\rangle$ in $Cu_{90}Ge_{10}$ possesses a bump at $\mathbf{p} = 0$; calculations show that this feature is isotropic in $\mathbf{p}$ and leads to a bump in the theoretical $dN(p_y,0)/dp_y$ curve (thinly drawn in Fig. 1). A calculation in which the p_x integration in Eq. (1) is restricted to the interval from minus to plus one half the distance ΓX in the Brillouin zone (rather than from $-\infty$ to $+\infty$) produces a practically identical bump in the derivative curve, thus excluding the possibility that the observed bump results

trivially from the line of integration intersecting the Fermi surface and the high-momentum (umklapp) components.[9] In Cu, on the other hand, a similarly restricted p_x integration yields an essentially zero derivative at low $\mathbf{p}$.

In Fig. 2, the contributions to $\langle\rho(\mathbf{p})\rangle$ from the host energy bands in the alloy and the Ge-related impurity band (lowest Δ_1 band; see inset) are given separately. Clearly, the impurity band hybridizes strongly with the conduction band (both are s-p-like), which results in a transfer of momentum density from the conduction to the impurity band. However, at low $\mathbf{p}$ there is an extra density amounting to $\approx 10\%$ at $\mathbf{p} = 0$, stemming from the delocalized s-p-like Ge states. The present 2D-ACAR results provide the first direct experimental evidence for the existence of this Ge-derived band and a verification of the KKR-CPA predictions in this respect.

We turn now to the FS radii and their disorder-induced smearing in the alloy. The derivative curve for Cu in Fig. 1 shows a peak at about $p_y = 5.4$ and a dip at $8.1 \times 10^{-3} mc$. The peak is caused by the discontinuity in $\rho(\mathbf{p})$ at the Fermi surface while the dip stems from the umklapp FS break in the (020) zone (at $ap/2\pi \approx 1.2$ in Fig. 2). As expected, both these features become broader in the alloy because of disorder broadening of levels, and, furthermore, the peak and the dip move respectively to higher and lower p_y values. These movements reflect the increase in the FS dimensions on alloy-
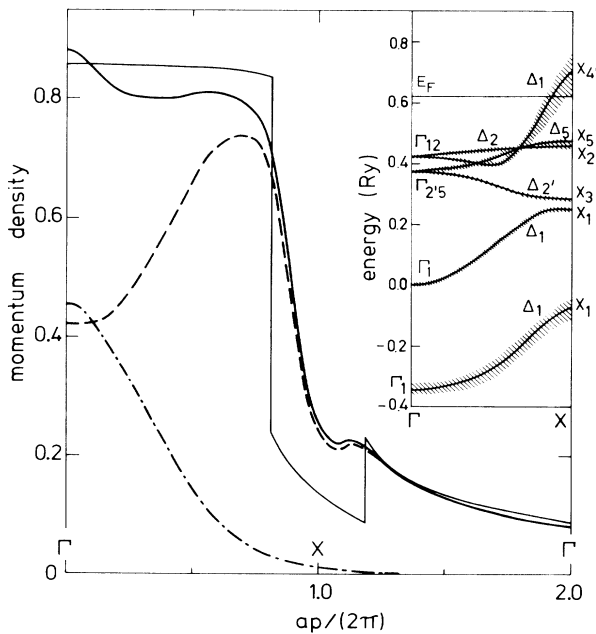

FIG. 2. Calculated momentum density along $\langle 100 \rangle$ in Cu (thin solid curve) and $Cu_{90}Ge_{10}$ (heavy solid curve). The latter is broken up into an $E \geq 0$ (dashed curve) and an $E < 0$ (dot-dashed curve) contribution. Inset: The band structure of $Cu_{90}Ge_{10}$ (Ref. 8).

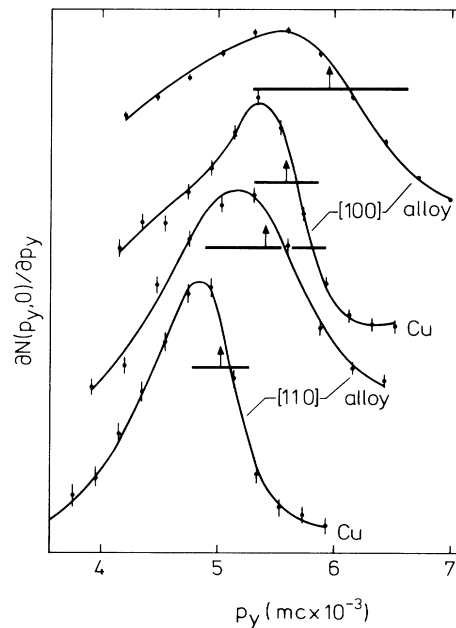FIG. 3. Derivatives $dN(p_y,0)/dp_y$ (in a limited range around k_F) for $(p_y,p_z) = ([010],[001])$ and $([1\bar{1}0],[001])$. The curves represent fits of the model described in the text. Arrows indicate the fitted Fermi radii, and heavy lines represent the smearing $2\Delta k_F$.

ing.

To obtain numerical values for the Fermi radii k_{100} and k_{110} and the damping of states at the Fermi surface in these two directions, we have performed a model calculation and fitted the results to the experimental derivative data. The model consists of a parabolic, but anisotropic, conduction band with dispersion relation

$$E_{\mathbf{k}} = k^2[C_0 + C_4(k_x^4 + k_y^4 + k_z^4) + C_6 k_x^2 k_y^2 k_z^2 + C_8(k_x^8 + k_y^8 + k_z^8)], \tag{2}$$

where k_x, etc., are the direction cosines of the wave vector $\mathbf{k}$, and $C_0, \ldots, C_8$ are still to be determined. Furthermore, it is assumed that the spectral momentum density is a Lorentzian with halfwidth Γ which describes a possible damping due to electron scattering. Integration of this spectral momentum density with respect to E up to E_F yields a "fuzzy" model momentum density

$$\rho(\mathbf{p}) = \pi^{-1} \arctan[(E_F - E_{\mathbf{k}})/\Gamma] + \tfrac{1}{2}. \tag{3}$$

Here $\mathbf{p} = \hbar \mathbf{k}$ with $\hbar = 1$ and Umklapp components are neglected. Before fitting of this model to the data, the coefficients $C_0, \ldots, C_8$ which describe the shape of the Fermi surface were determined by fitting of the FS resulting from Eq. (2) to the Halse-Cu7 FS[10] with an accuracy better than 0.3% within the angular region of interest. The fitted FS is used in the analysis of both the Cu and the alloy data. $N(p_y, p_z)$ is then obtained from Eqs. (1)–(3). After convolution with the instrumental resolution, $N(p_y, p_z)$ is differentiated, and the result is fitted to the data over the range $0.75 k_F < p_y < 1.2 k_F$. Five parameters, E_F, Γ, the height and slope of a linear background (to account for the derivative of the core and 3D contribution over this limited range), and a scale factor, are determined so as to minimize the residue of the fit. k_{100} and k_{110} are then readily obtained from E_F with Eq. (2), while the smearing Δk_F follows from $\Delta k_F = \Gamma/(dE/dk_y)$. Figure 3 shows that our fits are excellent in all cases. The FS smearing obtained for Cu is somewhat greater than the instrumental resolution, which is reasonable since most imperfections in the model [e.g., nonconstancy of $\rho(\mathbf{p})$ within the FS, neglect of many-body enhancement effects] will result in an increase of the fitted value of Γ.

Table II compares our results with the Halse-Cu7 radii in Cu and with the KKR-CPA calculations of Prasad and Bansil in $Cu_{91}Ge_9$.[8] A few remarks are in order. First, our precision of k_{100} and k_{110} for Cu is only a factor of 2 worse than the 0.2% accuracy of the dHvA radii. This was made possible by the a priori knowledge of the shape (not size) of the FS of Cu; otherwise, a 1% to 2% precision would have been more realistic.[11] The accuracy with which k_{110} has been determined is greater than that of k_{100} because of the flatness of the FS in the $\langle 110 \rangle$ direction. Secondly, in the alloy the value for k_{100} is in good agreement with the CPA predictions; the measured k_{110} is somewhat larger than the theoretical value. These results are in line with much lower-resolution angle-resolved photoemission measurements[12] and early positron-annihilation experiments.[13,14] Recent low-resolution point-geometry positron measurements[15] tend to give lower values. Finally, the electronic damping in the alloy was obtained by correction of the values of Δk_F shown in Fig. 3 for the instrumental resolution as derived from the Cu measurements (the positron disorder damping can be neglected[16]). The measured damping is about 50% larger than the KKR-CPA prediction, but this difference may be overestimated because of the use of the Cu7 FS shape also in the alloy. We consider the preceding agreement between theory and experiment with respect to radii and dampings to be satisfactory, given the inherent uncertainties in first-principles electronic structure calculations.

TABLE II. Fermi radii and disorder smearing of the Fermi surface (both in units of $10^{-3}mc = 2.5896$ nm^{-1}) in the $\langle 100 \rangle$ and $\langle 110 \rangle$ directions in Cu and $Cu_{91}Ge_9$.

| | Cu | | $Cu_{91}Ge_9$ | |
	Present work	dHvA (Ref. 10)	Present work	Theory[a]
k_{100}	5.58 ± 0.02	5.58 ± 0.01	5.94 ± 0.10	5.93
k_{110}	5.03 ± 0.02	5.01 ± 0.01	5.42 ± 0.03	5.32
Δk_{100}[b]	$\cdots$	$\cdots$	0.5 ± 0.1	0.35
Δk_{110}[b]	$\cdots$	$\cdots$	0.4 ± 0.1	0.23

[a]Values obtained from Ref. 8 by interpolation.

[b]Δk_F is half the full width of the smearing function.

[1]See, e.g., S. Wakoh, in *Positron Annihilation*, edited by R. R. Hasiguti and K. Fujiwara (Japan Institute of Metals, Sendai, 1979), p. 49; P. E. Mijnarends and A. Bansil, *ibid.*, p. 657.

[2]See, e.g., F. Sinclair, W. S. Farmer, and S. Berko, in *Positron Annihilation*, edited by P. G. Coleman, S. C. Sharma, and

L. M. Diana (North-Holland, Amsterdam, 1982), p. 322.

[3]P. Zwart, L. P. L. M. Rabou, G. J. Langedijk, A. P. Jeavons, A. P. Kaan, H. J. M. Akkerman, and P. E. Mijnarends, in *Positron Annihilation,* edited by P. C. Jain, R. M. Singru, and K. P. Gopinathan (World Scientific, Singapore, 1985), p. 297.

[4]A. P. Jeavons, Nucl. Instrum. Methods **156**, 41 (1978).

[5]A. Bansil, R. S. Rao, P. E. Mijnarends, and L. Schwartz, Phys. Rev. B **23**, 3608 (1981).

[6]The Cu and Ge muffin-tin potentials are identical to those used in our earlier work on CuGe alloys in R. Prasad and A. Bansil, Phys. Rev. Lett. **48**, 113 (1982).

[7]The inclusion of the positron spatial distribution will mainly reduce the high-momentum components of $\rho(\mathbf{p})$, but this is not expected to change the present considerations which focus on the relatively larger effects of alloying on $\rho(\mathbf{p})$. Similarly, the facts that $\langle\rho(\mathbf{p})\rangle$ is calculated for 10% Ge while the samples contain 9% Ge and that we have ignored electron-positron enhancement effects in the calculations are unimportant for the present discussion.

[8]See Prasad and Bansil, Ref. 6.

[9]S. Berko and J. S. Plaskett, Phys. Rev. **112**, 1877 (1958).

[10]M. R. Halse, Philos. Trans. Roy. Soc. London, Ser. A **265**, 507 (1969).

[11]Application of a locally spherical model to our Cu data yields $k_{100}=5.53$ and $k_{110}=5.00$, both in units of $10^{-3}mc$; the corresponding numbers for $Cu_{91}Ge_9$ are 5.78 and 5.44.

[12]A. Bansil, R. S. Rao, R. Prasad, H. Asonen, and M. Pessa, J. Phys. F **14**, 273 (1984).

[13]J. G. McLarnon and D. L. Williams, J. Phys. Soc. Jpn. **43**, 1244 (1977).

[14]T. Suzuki, M. Hasegawa, and M. Hirabayashi, Appl. Phys. **5**, 269 (1974).

[15]L. M. Pecora and A. C. Ehrlich, Phys. Rev. B **32**, 708 (1985).

[16]P. E. Mijnarends and A. Bansil, in Ref. 3, p. 58.